HHS Public Access

Author manuscript

Kidney Int. Author manuscript; available in PMC 2023 March 30.

Published in final edited form as:

Kidney Int. 2022 June ; 101(6): 1216–1231. doi:10.1016/j.kint.2021.12.031.

Inhibition of endoplasmic reticulum stress signaling rescues cytotoxicity of human apolipoprotein-L1 risk variants in *Drosophila*

Lea Gerstner[1,4], **Mengmeng Chen**[1,4], **Lina L. Kampf**[1], **Julian Milosavljevic**[1], **Konrad Lang**[1], **Ronen Schneider**[2], **Friedhelm Hildebrandt**[2], **Martin Helmstädter**[1], **Gerd Walz**[1,3], **Tobias Hermle**[1]

[1]Renal Division, Department of Medicine, Faculty of Medicine and Medical Center–University of Freiburg, Freiburg, Germany

[2]Renal Division, Department of Medicine, Boston Children's Hospital, Harvard Medical School, Boston, Massachusetts, USA

[3]Signalling Research Centres BIOSS and CIBSS, University of Freiburg, Freiburg, Germany

Abstract

Risk variants of the apolipoprotein-L1 (*APOL1*) gene are associated with severe kidney disease, putting homozygous carriers at risk. Since *APOL1* lacks orthologs in all major model organisms, a wide range of mechanisms frequently in conflict have been described for *APOL1*-associated nephropathies. The genetic toolkit in *Drosophila* allows unique *in vivo* insights into disrupted cellular homeostasis. To perform a mechanistic analysis, we expressed human *APOL1* control and gain-of-function kidney risk variants in the podocyte-like garland cells of *Drosophila* nephrocytes and a wing precursor tissue. Expression of *APOL1* risk variants was found to elevate endocytic function of garland cell nephrocytes that simultaneously showed early signs of cell death. Wild-type APOL1 had a significantly milder effect, while a control transgene with deletion of the short BH3 domain showed no overt phenotype. Nephrocyte endo-lysosomal function and slit diaphragm architecture remained unaffected by *APOL1* risk variants, but endoplasmic reticulum (ER) swelling, chaperone induction, and expression of the reporter *Xbp1*-EGFP suggested an ER stress response. Pharmacological inhibition of ER stress diminished APOL1-mediated cell death and direct ER stress induction enhanced nephrocyte endocytic function similar to expression of APOL1 risk variants. We confirmed APOL1-dependent ER stress in the *Drosophila* wing precursor where silencing the IRE1-dependent branch of ER stress signaling by inhibition with *Xbp1*-RNAi abrogated cell death, representing the first rescue of APOL1-associated cytotoxicity

Correspondence: *Tobias Hermle, Renal Division, Department of Medicine, University Medical Center Freiburg, Hugstetter Strasse 55, 79106 Freiburg, Germany.* tobias.hermle@uniklinik-freiburg.de.

[4]LG and MC contributed equally.

AUTHOR CONTRIBUTIONS

LG, MC, TH, KL, and JM performed experiments in *Drosophila*. MC, LLK, LG, RS, and TH performed cDNA cloning and immunofluorescence studies in cell lines by confocal microscopy. GW and FH critically reviewed the manuscript. MH performed electron microscopy. TH conceived of and directed the study. TH wrote the manuscript. LG prepared the data figures. The manuscript was critically reviewed by all the authors.

DISCLOSURE

All the authors declared no competing interests.

in vivo. Thus, we uncovered ER stress as an essential consequence of *APOL1* risk variant expression *in vivo* in *Drosophila*, suggesting a central role of this pathway in the pathogenesis of *APOL1*-associated nephropathies.

Keywords

APOL1; *Drosophila* ; endoplasmic reticulum stress; focal segmental glomerular sclerosis; nephrocyte; podocyte

African ancestry is associated with a significantly higher prevalence of end-stage kidney disease.[1] Genetic studies identified 2 risk variants (termed G1 and G2) within the gene apolipoprotein-L1 (*APOL1*) that account for ≈70% of the excess risk.[2-7] The risk variants are exceedingly common as heterozygous presence confers protection against sleeping sickness.[8,9] In the homozygous state, the risk variants are associated with debilitating glomerular disease,[10] such as global or focal segmental glomerular sclerosis[10] and HIV-associated or severe acute respiratory syndrome coronavirus 2 (SARS-CoV-2)–associated collapsing focal segmental glomerular sclerosis.[11] Homozygous carriers, estimated at >70 million worldwide,[7] carry a lifetime risk for *APOL1*-associated kidney disease of ~15%.[10] Targeted therapies are unavailable, and the pathogenesis of *APOL1*-associated nephropathies remains a conundrum. The renal pathogenesis appears independent from circulating APOL1[12,13] but linked to the gene's intracellular function. Kidneys from donors carrying the *APOL1* risk variants showed reduced allograft survival in wild-type recipients,[14] despite the presence of wild-type APOL1 in the recipient's circulation. However, because orthologs are restricted to higher primates, the cell-autonomous function of APOL1 is poorly understood. *APOL1* G1 and G2 variants are considered hypermorphic alleles because *APOL1* is dispensable in most mammals and human subjects carrying APOL1 null alleles showed no renal anomalies.[15] Loss-of-function hypotheses were proposed,[16-18] but the currently prevalent hypothesis involves a dose-dependent deleteriousness of *APOL1* that is subject to modifiers,[19] requiring second hits. The latter include environmental factors[20] and inflammatory processes, because interferons and toll-like receptor agonists elevate expression of *APOL1*.[21] Supporting the gain-of-function hypothesis, *APOL1* risk alleles entail cytotoxicity. Necrosis, pyroptosis, apoptosis, and autophagic cell death have been described on expression of *APOL1* risk variants.[22-27] Mice with transgenic expression of human *APOL1* recapitulated aspects of human disease, such as proteinuria and podocyte depletion.[27-29] The proposed mechanisms of *APOL1*-associated renal disease include autophagic flux,[26,27] impaired endocytosis,[30-32] mitochondrial dysfunction,[33,34] downregulation of miR193a,[18] coactivation of integrins with soluble urokinase plasminogen activator receptor (suPAR),[35] Na^+/Ca^{2+}-influx,[36] activation of protein kinases,[22,37] and endoplasmic reticulum (ER) stress.[38] The plethora of reported abnormalities makes it difficult to identify the key signaling pathways. Transgenic expression of *APOL1* in *Drosophila* pericardial nephrocytes[30,31] resulted in an initial increase of endocytic nephrocyte function and nephrocyte death on prolonged expression in adult flies. However, the underlying mechanisms remained unclear. Herein, we employed transgenic expression of *APOL1* variants in *Drosophila* larvae and performed a mechanistic analysis using garland

cell nephrocytes and wing imaginal discs. We identified ER stress induction as the essential cause of *APOL1*-dependent cytotoxicity in *Drosophila*.

METHODS

Fly strains and husbandry

Flies were reared on standard food at room temperature, 18 °C, 25 °C, or 29 °C, as indicated. Overexpression and transgenic RNA interference (RNAi) studies were performed using the upstream activating sequence (UAS)/*GAL4* system. Fly stocks used in this study are described in Supplementary Table S1.

Transgenesis of human APOL1

To generate *APOL1*-expressing transgenic flies, we cloned human *APOL1* full-length cDNA (GE Dharmacon; GenBank: BC112943.1) into pUASg-attB (from K. Basler). The DNA was injected into flies expressing phiC31 integrase under vasa promoter with an attP landing site (86F8) by BestGene. Primer sequences see Supplementary Table S2. Hemagglutinin (HA) tags are present in all *APOL1* transgenes unless otherwise indicated. New lines generated for this study are G0-*APOL1*-no tag, G0-*APOL1*, G2-*APOL1*-no tag, G2-*APOL1*, G1-*APOL1*, **Δ**BH3-G2-*APOL1*, and **Δ**BH3-G2-*APOL1*-no tag. Genetic combinations were achieved by standard crosses.

Fluorescent tracer uptake

Fluorescent tracer uptake in nephrocytes to evaluate nephrocyte function was performed as previously described.[39] Briefly, nephrocytes were dissected in phosphate-buffered saline (PBS) and incubated with fluorescein isothiocyanate (FITC)–albumin (Sigma) or Texas Red–avidin (Thermofisher) for 30 seconds. After a fixation step of 5 minutes in 8% paraformaldehyde, cells were rinsed in PBS and exposed to Hoechst 33342 (1:1000) for 20 seconds and mounted in ROTI-Mount (Carl Roth). Cells were imaged using a Zeiss LSM 880 laser-scanning microscope. Quantitation of fluorescent tracer uptake was performed with ImageJ software. The results are expressed as a ratio to a control experiment with flies carrying the (heterozygous) *GAL4* transgene but no UAS that was done in parallel.

For the fluorescent double tracer uptake to study processing of endocytic cargo, nephrocytes were dissected in Schneider's medium and incubated with FITC-albumin for 30 seconds. Washing steps with cold PBS were followed by a 45-minute chase period in Schneider's medium at 25 °C and Texas Red–albumin was applied and incubated for 3 minutes. After fixation for 5 minutes in 8% paraformaldehyde, cells were rinsed in PBS and exposed to Hoechst 33342 (1:1000) for 20 seconds and mounted in ROTI-Mount (Carl Roth). Image quantitation was performed using ImageJ software.

LysoTracker assay

For Lysotracker labeling, larvae were dissected, incubated in PBS containing 0.25 μM Lysotracker (LysoTracker Red DND-99; Thermofisher; L7528) for 5 minutes before immediate live cell imaging on a Zeiss LSM 880 laser-scanning microscope. Image processing was done by ImageJ and GIMP software.

Immunoblotting of *Drosophila* tissue

For immunoblotting from *Drosophila* tissue, we dissected 30 to 40 wing imaginal discs per genotype from third instar larvae expressing *APOL1* variants for 24 hours using *ptc-GAL4*; *GAL80*^{ts}. The explanted tissue was incubated for 15 minutes in ice-cold immunoprecipitation lysis buffer containing protease inhibitor (Merck/Roche). After sonication, samples were centrifuged for 15 minutes at 14,000 rpm and loaded onto a 10% sodium dodecylsulfate–polyacrylamide gel. Protein was transferred to polyvinylidene difluoride membranes (Millipore/Thermofisher). *APOL1*-HA transgene expression was detected using rat anti-HA (1186742300; Merck/Roche); mouse anti-tubulin (E7; DSHB) served as loading control.

TUNEL assay and immunofluorescence

For immunofluorescence, nephrocytes or wing imaginal discs were dissected, fixed for 20 minutes in 4% paraformaldehyde, blocked in 5% albumin for 1 hour, incubated in primary antibodies overnight, and in Alexa fluorophore–conjugated secondary antibodies (Invitrogen) for 2 hours before mounting in ROTI-Mount (Carl Roth). Primary antibodies are described in Supplementary Table S3. For terminal deoxynucleotidyl transferase–mediated dUTP nick end-labeling (TUNEL), larvae were dissected, fixed in 4% paraformaldehyde for 15 minutes, and stained according to the manufacturer's instructions (*In situ* Cell Death Detection Kit, Fluorescein; Roche catalog number 11684795910). For Texas Red–avidin colabeling, tracer uptake was performed before the fixation step, followed by TUNEL. For imaging, a Zeiss LSM 880 laser-scanning microscope was used. Image processing was done by ImageJ and GIMP software.

Drosophila drug feeding

For short-term pharmacologic ER stress inhibition, late second instar larvae were raised in liquid food (H_2O with 5% sucrose, 10% yeast extract, and 0.5% propionic acid) containing 4 mM 4-phenylbutyric acid (4-PBA) as an ER stress inhibitor for 24 hours at 25 °C followed by dissection and staining according to standard procedure. For prolonged ER stress inhibition, early second instar larvae were raised on grape juice plates (H_2O with 25% grape juice, 2.15% agar, 1.25% sugar, and 0.2% nipagin) with yeast containing 4 mM 4-PBA for 48 hours at 29 °C followed by dissection of the adult nephrocytes and staining after eclosure. For short-term ER stress induction, early third instar larvae were exposed to tunicamycin, 10 μg/ml, in liquid food for 5 hours at 25 °C followed by dissection and staining.

Electron microscopy

For transmission electron microscopy, nephrocytes were dissected and fixed in 4% paraformaldehyde and 0.5% glutaraldehyde in 0.1 M cacodylate buffer, embedded in 2% low melting agarose (Invitrogen), postfixed in 1% osmium tetroxide, and incubated in 1% uranyl acetate. Dehydration was performed using ethanol. After embedding in Durcupan resin, ultrathin sections were cut using a UC7 Ultramicrotome (Leica). Grids were imaged using a Leo 912 transmission electron microscope (Zeiss).

Plasmids

APOL1 full-length cDNA was subcloned after polymerase chain reaction (GE Dharmacon; GenBank: BC112943.1). This clone carries 3 single-nucleotide polymorphisms (E150K, M228I, and R255K) that represent one of the most common haplotypes, thus deviating from the reference that actually is a minor *APOL1* haplotype. We did not revert the clone to E150, which predominates in Africa. This might blunt risk variant toxicity in our transgenes.[40] The mutation reflecting G2-*APOL1* was generated using Quik change II XL site-directed mutagenesis kit (Agilent Technologies). G1-*APOL1* and other modifications were generated by polymerase chain reaction followed by Gibson Assembly (New England Biolabs) and LR reactions (LR clonase II Enzyme Mix; Thermofisher). Primers are shown in Supplementary Table S2.

Statistical analysis

Paired *t* test was used to determine the statistical significance between 2 interventions. Analysis of variance followed by Dunnett's correction (unless otherwise indicated) was used for multiple comparisons (GraphPad Prism software). Asterisks indicate significance as follows: $*P < 0.05$, $**P < 0.01$, $***P < 0.001$, and $****P < 0.0001$. A statistically significant difference was defined as $P < 0.05$. Error bars indicate SD.

RESULTS

Expression of human *APOL1* risk variants increases garland cell nephrocyte function and induces cell death indicated by TUNEL positivity

Nephrocytes in *Drosophila* form slit diphragms across membrane invaginations representing a podocyte model for genetic kidney diseases.[39,41] Transgenesis of *APOL1* risk variants in adult pericardial nephrocytes was shown to result in a short-term increase of nephrocyte function but functional decline and cell death with prolonged expression.[30,31] To explore the function of *APOL1*, we generated transgenic *Drosophila* lines expressing wild-type G0-*APOL1* and the risk variants G1 (p.S342G and p.I384M) and G2 (del: N388/Y389), each carrying a single-copy C-terminal influenza HA tag (Figure 1a; HA tags are present in all *APOL1* transgenes unless otherwise indicated). An identical landing site (ZH-86Fb) using phiC31 integrase was chosen for all transgenes to ensure equal expression, which was further confirmed by immunoblotting (Supplementary Figure 1A). A G2-*APOL1* variant that lacks 9 amino acids (del: L158-Q166) in the BCL2 homology domain 3[26] (ΔBH3-G2), which is part of the protein's pore forming domain, served as control protein (Figure 1a). Because expression of our transgenes using *prospero-GAL4* and *Dorothy*-GAL4 resulted in early lethality (data not shown), we employed *Hand-GAL4* or *dKlf15-GAL4* that directed low-level expression in nephrocytes, allowing eclosure of phenotypically normal adults for all transgenes. We studied garland cell nephrocyte function in third instar larvae based on FITC-albumin endocytosis[39] and confirmed a significantly increased function for this nephrocyte subset on expression of *APOL1* risk variants but not for the wild-type or the control protein (ΔBH3-G2-*APOL1*; Figure 1b and c; FITC-albumin/HA colabeling using *dKlf15-GAL4*; Supplementary Figure S1B). To study the impact of *APOL1* on nephrocyte slit diaphragm formation, we stained the slit diaphragm proteins Sns (nephrin) and Kirre (NEPH1). We occasionally and variably observed few intracellular vesicles of the slit

diaphragm proteins (Supplementary Figure S1C-G"), but otherwise noted no overt alteration of cellular slit diaphragm architecture for expression of all *APOL1* variants (Figure 1d-h). Because *APOL1* risk variant expression is known to entail cell death,[2] we performed TUNEL that was previously employed to detect nephrocyte cell death.[39,41] We observed a fraction of TUNEL-positive nephrocytes in third instar larvae that express *APOL1* variants, predominantly on risk variant expression (Figure 1i-m). Quantification of TUNEL-positive nuclei confirmed a significantly higher positivity for the risk variants alone (Figure 1n). In larval nephrocytes, TUNEL-positive and TUNEL-negative nephrocytes exhibited similar uptake of Texas Red–avidin, suggesting these still functional nephrocytes showed an early stage of cell death (Figure 1o-r).

Staining adult nephrocytes expressing *APOL1* variants under *dKlf15-GAL4*, we detected a significantly reduced number of nephrocytes exclusively for the risk variants compared with ΔBH3-G2-*APOL1* (Supplementary Figure S2A-D‴; quantitation in Supplementary Figure S2E). Only few individual nephrocytes lacked transgene expression in **Δ**BH3-G2-*APOL1* and G0-*APOL1* but transgene expressing cells were mostly lacking for the risk variants (Supplementary Figure S2F). Taken together, we conclude that *APOL1* risk variants cause cell death for a fraction of nephrocytes during the pupal stage, whereas few cells persisted after eclosion managing to escape cell death by downregulation of the transgene expression, which depends on the *dKlf15*-promoter.

Expression of human *APOL1* risk variants does not result in defective endolysosomal processing

Defective endolysosomal acidification was described on transgenic *APOL1* expression in adult *Drosophila*.[30,31] To explore a role for acidification in our model, we performed lysotracker staining, but we observed no significant difference in lysotracker intensity between control and *APOL1* variants (Figure 2a-e; quantitation in Figure 2f). Then, we stained the endosomal compartment markers Rab5 and Rab7, but the characteristic pattern of early/late endosomes remained unaltered by G2-*APOL1* (Supplementary Figure S3A-B″). We costained G0-/G1-/G2/**Δ**BH3-G2-APOL1 in nephrocytes but observed colocalization neither with early (Supplementary Figure S3C-F″) nor late endosomal markers (Supplementary Figure S4A-D″), indicating absence of *APOL1* variants from early/late endosomes. To study endolysosomal cargo processing directly, we applied endocytic tracers FITC-albumin and Texas Red–albumin *ex vivo*. After an initial tracer pulse of FITC-albumin, nephrocytes were chased for 45 minutes following a second pulse with Texas Red–albumin. Indicating endolysosomal processing, the tracer signals were sharply separated in control nephrocytes (Figure 2g). Inhibition of endolysosomal acidification by V-ATPase inhibitor bafilomycin resulted in slower processing and consecutively enhanced colocalization of both tracer fractions (Figure 2h). In contrast, G0/G2-*APOL1* constructs did not interfere with cargo processing, and separation became even more apparent on expression of the risk variant G2-*APOL1* (Figure 2i and j; quantitation in Figure 2k). Consequently, we found no evidence for an *APOL1*-mediated alteration of endolysosomal function.

APOL1 expression induces ER swelling in *Drosophila* nephrocytes

To explore alternative mechanisms, we performed electron microscopy that revealed normal slit diaphragms (Figure 3b-d; control in Figure 3a). Although defective autophagic flux has been reported with transgenic expression of *APOL1* in mice,[27] we observed no autophagosomes using electron microscopy. Instead, we noted mild swelling of the nephrocytes' ER on expression of G0-*APOL1* (Figure 3f; control in Figure 3e). ER swelling was significantly enhanced by expression of *G1-APOL1* (Figure 3g), and strongest in G2-*APOL1* (typical cell in Figure 3h, example for more severe swelling in Figure 3i, and quantitation in Figure 3j). This represents a strong indication of ER stress induction, through risk variant expression in particular. A similar connection was reported in immortalized podocytes.[38]

APOL1 variants localize to the ER and induce ER stress in *Drosophila* nephrocytes

To explore the role of the *APOL1* variants, we determined their subcellular localization. Costaining HA-tag with the ER marker calnexin, we observed strong colocalization for all *APOL1* variants in a near-identical staining pattern (Supplementary Figure S5B-E″; nonexpressing cell in Supplementary Figure S5A-A″). In almost all animals, the vast majority of APOL1-HA signal seemed to originate from the ER, whereas a minute fraction in the cytosol is possible. This is compatible with localization of APOL1 in human cells, where APOL1 protein was mainly detected in the ER,[33,42-44] aside from other compartments,[2] such as the plasma membrane.[44] Of note, careful analyses,[44] including most recent studies[45] that differentiate between APOL1 and APOL2, indicate a luminal ER topology. Staining the HA-tagged G2-APOL1 with an anti-APOL1 antibody revealed an indistin-guishable staining pattern (Supplementary Figure S6A-A″), suggesting the HA staining reflects APOL1. We further generated several transgenic *APOL1* variants lacking the C-terminal HA-tag, which equally colocalized with calnexin (Supplementary Figure S6B-D″). The HA-tag therefore does not affect the subcellular localization.

Because the subcellular localization of APOL1 variants seemed mostly restricted to the ER, causing ER swelling and cell death in risk variants, we hypothesized that APOL1 variants may induce an ER stress response in *Drosophila* nephrocytes. ER stress signaling prevents accumulation of unfolded protein by promoting ER homeostasis and survival through enhanced expression of chaperone proteins, whereas unmitigated ER stress activation induces cell death (schematic in Supplementary Figure S7). Upregulation of the ER marker and chaperone protein disulfide-isomerase (PDI) is an indicator of the ER stress activation.[46] We stained PDI in nephrocytes expressing *APOL1* control and risk variants and compared the fluorescence intensity. Confirming ER stress induction in nephrocytes, we observed a significantly enhanced intensity exclusively for the risk variants (Figure 4a-d″; quantitation in Figure 4e). Although cell death represents a canonical consequence of ER stress, we asked whether enhanced FITC-albumin endocytosis, previously only reported for Cubilin overexpression,[47] also follows ER stress induction. We induced ER stress by feeding early third instar *Drosophila* larvae for 5 hours with liquid food containing tunicamycin (10 μg/ml), which significantly increased nephrocyte function based on the FITC-albumin assay (Figure 4f and g; quantitation in Figure 4h), whereas slit diaphragms remained undisturbed (Figure 4i-i″). Thus, ER stress induction phenocopies *APOL1* risk variant expression.

APOL1 expression induces ER stress preceding cell death in *Drosophila* wing discs

To explore if the ER stress induction is specific for nephrocytes and confirm the effect in an epithelial model that enables recording of relative ER stress side by side within the same animal,[46,48] we employed *Drosophila* wing precursor tissue. On expression of G0-*APOL1* in a narrow strip within the wing imaginal disc using *ptc-GAL4*, we observed mild upregulation of PDI as an indication of ER stress (Figure 5a-a‴). Thus, *APOL1*-mediated ER stress is not limited to nephrocytes. Within the G0-*APOL1* expression domain, induction of cell death was detected by staining of cleaved caspase-3 (Figure 5a-a‴), confirming that expression of wild-type *APOL1* suffices to induce ER stress and cell death. However, overexpression of the renal risk variants *G1-APOL1* (Figure 5b-b‴) and *G2-APOL1* (Figure 5c-c‴) caused a markedly stronger upregulation of PDI and cell death, whereas the control transgene (**Δ**BH3-G2) had no effect (Figure 5d-d‴; quantitation for PDI/cleaved caspase-3 in Figure 5e and f). Studying adult wing phenotypes of G0-*APOL1* and the renal risk variants was precluded by pupal lethality using *ptc-GAL4*, even with lower expression at 18 °C. In contrast, animals expressing **Δ**BH3-G2-*APOL1* developed normally and formed regular wings (Supplementary Figure S8A and B). Expression with *1096-GAL4* that stimulated diffuse G0-/G2-*APOL1* expression throughout the wing disc resulted in adult animals lacking wings (Supplementary Figure S8C; expression of G2-*APOL1*, not shown for G0-*APOL1*). To evaluate if ER stress precedes induction of cell death and occurs independently, we modified *GAL4*-dependent expression of *APOL1* variants by $GAL80^{ts}$, which blocks *GAL4*-dependent expression selectively at temperatures of <29 °C. We raised larvae at 25 °C and induced *APOL1* variant expression acutely through a temperature shift to 29 °C. **Δ**BH3-G2-*APOL1*, G0-*APOL1*, and G2-*APOL1* each were detectable after 24 hours, but only the renal risk variant G2-*APOL1* but not **Δ**BH3-G2-*APOL1* and G0-*APOL1* resulted in significant upregulation of PDI (quantification for PDI/cleaved caspase-3 in Supplementary Figure S9A-E). Shortterm expression of any of the *APOL1* variants lacked cell death. Significant cleaved caspase-3 became detectable after prolonged expression of G2-*APOL1* for 48 hours (Supplementary Figure S10A-D). This confirms that *APOL1*-dependent activation of ER stress precedes cell death.

ER stress induction on *G2-APOL1* causes *IRE1*-dependent ER stress

ER stress signaling is initiated by unfolded protein that buffers the chaperone binding-Ig protein (bip, CG4147). Bip dissociation from specific sensor proteins, such as inositol requiring enzyme 1 (*IRE1*), initiates the unfolded protein response[49] (schematic in Supplementary Figure S7). To test activation of the *IRE1*-mediated branch of the ER stress signaling pathway directly, we generated flies expressing G2-*APOL1* together with *Xbp1*–enhanced green fluorescent protein (EGFP).[50] Transgenic reporter *Xbp1*-EGFP employs *IRE1*-mediated alternative splicing of *Xbp1* that shifts the reading frame, and green fluorescent protein expression indicates activation of *IRE1*-dependent ER stress (Figure 6a). We focused exclusively on G2-*APOL1* in the wing as G1-*APOL1* showed extensive lethality with *ptc-GAL4*. EGFP was absent from the wing pouch under control conditions (Figure 6b) but became visible on induction of ER stress through silencing of *Drosophila bip* (Figure 6c). Similarly, expression of G2-*APOL1* strongly induced the expression of *Xbp1*-EGFP, specifically indicating a G2-*APOL1*–dependent activation of the *IRE1*-mediated ER

stress module (Figure 6d-d"). We further examined IRE1-mediated ER stress induction in nephrocytes and observed no significant increase of reporter activity for G0-*APOL1* compared with control cells (Figure 6e-e"; control in Figure 6h). In contrast, expression of the risk variants G1- and G2-*APOL1* significantly induced the *Xb1*-EGFP reporter that translocated to the nucleus (Figure 6f-g"; positive control in Figure 6i; quantitation in Figure 6j). This indicates that the *APOL1* risk variants specifically activate *IRE1*-dependent ER stress.

Treatment with ER stress inhibitor 4-PBA attenuates *APOL1*-dependent cytotoxicity in *Drosophila*

To test if pharmacologic inhibition of ER stress decreases cell death in connection with *APOL1* risk variants, we employed 4-PBA, a small molecule chemical chaperone and US Food and Drug Administration–approved drug. Late second instar G1- and G2-*APOL1*–expressing larvae were raised in liquid food that contained 4 mM 4-PBA or vehicle (H_2O) for 24 hours, followed by TUNEL labeling. On 4-PBA treatment, we observed a significant reduction of TUNEL positivity for G1-*APOL1* (Figure 7a and b; quantitation in Figure 7e), suggesting that cell death associated with G1 is a consequence of ER stress. For G2-*APOL1* expression, that causes a more variable extent of TUNEL positivity; we similarly observed a trend for a reduced TUNEL positivity, but in a range that was statistically not significant (Figure 7c and d; quantitation in Figure 7e). To examine if nephrocyte survival during G*2-APOL1* expression is improved by transient attenuation of ER stress, we studied nephrocyte numbers in adult animals with or without prolonged feeding with 4-PBA. Confirming improved survival, we observed a significantly increased number of nephrocytes after treatment with 4-PBA (Figure 7f-g"; quantitation of total number of adult nephrocytes in Figure 7h and number of G2-*APOL1*–expressing cells Figure 7i). Although 4-PBA strongly reduced G1-*APOL1*–dependent TUNEL positivity in larval nephrocytes (Figure 7e), this treatment was inefficient in rescuing adult nephrocyte numbers from the extensive toxicity of G1-*APOL1* (data not shown). The transient 4-PBA exposure that inevitably is suspended for 4 days by lack of feeding during the pupal stage appears to convey insufficient acute ER stress attenuation for the more intense toxicity of G1-*APOL1*. To assess if G2-*APOL1*–dependent ER stress induction can be treated by pharmacologic inhibition in the wing, we again applied ER stress inhibitor 4-PBA short-term in larvae. On 4-PBA-treatment, we observed mild attenuation of PDI induction that was sufficient to significantly reduce caspase 3–dependent cell death in wing cells (Figure 7j-k‴; quantitation in Figure 7l). These data confirm that ER stress is essential for G2-*APOL1*–dependent toxicity and show a potential treatment strategy.

Silencing *Xbp1* rescues *APOL1*-dependent cytotoxicity in the *Drosophila* wing disc

To test if the *IRE1* module is critical for *APOL1*-mediated cytotoxicity, we inhibited this branch of ER stress concomitant with G2-*APOL1* and G1-*APOL1* expression in the wing disc. Coexpression of *Xbp1*-RNAi (Figure 8a-a‴/Figure 8c-c‴) but not control RNAi (green fluorescent protein; Figure 8b-b‴/Figure 8d-d‴) abrogated *APOL1*-dependent cleaved caspase-3 induction. This shows that *IRE1*-dependent ER stress induction is essential for cell death associated with either APOL1 risk variant. Although elevated expression of PDI remained detectable albeit at a lower level, this most likely indicates

that *APOL1* expression also triggers ER stress through another sensor protein, but silencing 1 of 3 unfolded protein response sensors seemed sufficient to abrogate cell death. The lesser extent of cell death associated with wild-type G0-*APOL1* was equally blocked on *Xbp1* silencing, indicating that wild-type and risk variants both induce *Xbp1*-dependent ER stress but at various degrees (Figure 8e-f‴; quantitations in Figure 8g and h). Coexpression of *Xbp1*-RNAi with *ptc-GAL4* further reverted lethality of G1-/G2-*APOL1*. In contrast to control conditions, attenuation of ER stress allowed expression of *APOL1* variants at 25 °C and eclosure of adults with phenotypically normal wings (Supplementary Figure S8D and E). Taken together, these data imply inhibition of *IRE1*-dependent ER stress as successful rescue for cytotoxicity of *APOL1* transgene expression *in vivo*.

DISCUSSION

Herein, we explore the role of transgenic *APOL1* renal risk variants in *Drosophila*. In the podocyte-like garland cell nephrocytes, we observed regular slit diaphragm formation, but gain of nephrocyte endocytic function and cell death specifically for the renal risk variants. In our model, we detected ER stress, indicated by pronounced ER swelling and chaperone upregulation. We specifically identified *Xbp1*-dependent ER stress induced by *APOL1* risk variants. Cell death caused by *APOL1* risk variants was blunted on pharmacologic attenuation of ER stress. Induction of ER stress by tunicamycin phenocopied *APOL1*-dependently enhanced nephrocyte function. We confirmed ER stress and cell death induction in the wing disc as an epithelial model that allows side-by-side comparison. Supporting a gain-of-function hypothesis, G0-*APOL1* entailed milder ER stress and cytotoxicity, being exceeded by the risk variants. More important, *Xbp1*-RNAi abrogated cell death caused by G0-/G1-/G2-*APOL1*, confirming ER stress induction as the essential step for *APOL1*-dependent cytotoxicity in *Drosophila*.

Misfolding of *APOL1* transgenes in *Drosophila* might cause ER stress. However, ER stress was also reported in human cells.[38] Furthermore, we observed significant phenotypic differences between wild-type and risk variants; our control transgene, lacking merely 9 amino acids in the pore-forming domain, had no similar impact. Thus, misfolding seems unlikely, rather suggesting a specific mechanism, possibly related to ion transport. APOL1 acts as a pH-dependent cation channel,[9,51] and most recent evidence reinforces the significance of this function.[52,53] Therefore, ER stress is likely an effect that occurs downstream of cation conductance, and further work is needed to elucidate the mechanisms. Targeting ER stress may become a therapeutic strategy in the future. Because chronic ER stress inhibition appears to harm podocytes,[54] a targeted approach will be required.

Defective endolysosomal acidification has previously been reported using *Drosophila* pericardial nephrocytes.[30,31] In contrast to ER stress that precedes cell death, this defect appeared to be limited to late adult stages when nephrocyte numbers were reduced. It is difficult to extrapolate between the different models, but defective acidification could be the consequence, rather than the cause, of decreased cellular viability.

In conclusion, our findings define a critical role for ER stress in *APOL1*-mediated cytotoxicity in the *Drosophila* model.

Supplementary Material

Refer to Web version on PubMed Central for supplementary material.

ACKNOWLEDGMENTS

We thank C. Meyer for excellent technical support and R. Nitschke, Life Imaging Centre, University of Freiburg, for help with confocal microscopy. We thank Severine Kayser for technical assistance with electron microscopy. We thank Giorgos Pyrowolakis, Anne Classen, Paul Hartley, Michael Köttgen, and Matias Simons for sharing transgenic *Drosophila* lines.

We thank the Developmental Studies Hybridoma Bank for antibodies. This research was supported by grants from the Deutsche Forschungsgemeinschaft to TH (HE 7456/3-1 and HE 7456/4-1) and project-ID 431984000–SFB 1453 (to TH and GW). LLK and JM were supported by the MOTI-VATE program of the Medical Faculty of the University of Freiburg. MC was supported by the China Scholarship Council. TH and KL acknowledge support from the Deutsche Gesellschaft für Innere Medizin.

REFERENCES

1. United States Renal Data System. 2016 USRDS Annual Data Report: Epidemiology of Kidney Disease in the United States. Bethesda, MD: National Institutes of Health, National Institute of Diabetes and Digestive and Kidney Diseases; 2016.
2. Friedman DJ, Pollak MR. APOL1 and kidney disease: from genetics to biology. Annu Rev Physiol. 2020;82:323–342. [PubMed: 31710572]
3. Genovese G, Friedman DJ, Ross MD, et al. Association of trypanolytic ApoL1 variants with kidney disease in African Americans. Science. 2010;329:841–845. [PubMed: 20647424]
4. Tzur S, Rosset S, Shemer R, et al. Missense mutations in the APOL1 gene are highly associated with end stage kidney disease risk previously attributed to the MYH9 gene. Hum Genet. 2010;128:345–350. [PubMed: 20635188]
5. Friedman DJ, Pollak MR. Apolipoprotein L1 and kidney disease in African Americans. Trends Endocrinol Metab. 2016;27:204–215. [PubMed: 26947522]
6. Beckerman P, Susztak K. APOL1: the balance imposed by infection, selection, and kidney disease. Trends Mol Med. 2018;24:682–695. [PubMed: 29886044]
7. Kruzel-Davila E, Skorecki K. Dilemmas and challenges in apolipoprotein L1 nephropathy research. Curr Opin Nephrol Hypertens. 2019;28:77–86. [PubMed: 30431460]
8. Perez-Morga D, Vanhollebeke B, Paturiaux-Hanocq F, et al. Apolipoprotein L-I promotes trypanosome lysis by forming pores in lysosomal membranes. Science. 2005;309:469–472. [PubMed: 16020735]
9. Thomson R, Finkelstein A. Human trypanolytic factor APOL1 forms pH-gated cation-selective channels in planar lipid bilayers: relevance to trypanosome lysis. Proc Natl Acad Sci U S A. 2015;112:2894–2899. [PubMed: 25730870]
10. Dummer PD, Limou S, Rosenberg AZ, et al. APOL1 kidney disease risk variants: an evolving landscape. Semin Nephrol. 2015;35:222–236. [PubMed: 26215860]
11. Velez JCQ, Caza T, Larsen CP. COVAN is the new HIVAN: the reemergence of collapsing glomerulopathy with COVID-19. Nat Rev Nephrol. 2020;16:565–567. [PubMed: 32753739]
12. Bruggeman LA, O'Toole JF, Ross MD, et al. Plasma apolipoprotein L1 levels do not correlate with CKD. J Am Soc Nephrol. 2014;25:634–644. [PubMed: 24231663]
13. Kozlitina J, Zhou H, Brown PN, et al. Plasma levels of risk-variant APOL1 do not associate with renal disease in a population-based cohort. J Am Soc Nephrol. 2016;27:3204–3219. [PubMed: 27005919]
14. Reeves-Daniel AM, DePalma JA, Bleyer AJ, et al. The APOL1 gene and allograft survival after kidney transplantation. Am J Transplant. 2011;11:1025–1030. [PubMed: 21486385]
15. Johnstone DB, Shegokar V, Nihalani D, et al. APOL1 null alleles from a rural village in India do not correlate with glomerulosclerosis. PLoS One. 2012;7:e51546. [PubMed: 23300552]

16. Kotb AM, Simon O, Blumenthal A, et al. Knockdown of ApoL1 in zebrafish larvae affects the glomerular filtration barrier and the expression of nephrin. PLoS One. 2016;11:e0153768. [PubMed: 27138898]
17. Kumar V, Singhal PC. APOL1 and kidney cell function. Am J Physiol Renal Physiol. 2019;317:F463–F477. [PubMed: 31241995]
18. Kumar V, Paliwal N, Ayasolla K, et al. Disruption of APOL1-miR193a axis induces disorganization of podocyte actin cytoskeleton. Sci Rep. 2019;9:3582. [PubMed: 30837512]
19. Zhang JY, Wang M, Tian L, et al. UBD modifies APOL1-induced kidney disease risk. Proc Natl Acad Sci U S A. 2018;115:3446–3451. [PubMed: 29531077]
20. Langefeld CD, Comeau ME, Ng MCY, et al. Genome-wide association studies suggest that APOL1-environment interactions more likely trigger kidney disease in African Americans with nondiabetic nephropathy than strong APOL1-second gene interactions. Kidney Int. 2018;94:599–607. [PubMed: 29885931]
21. Zhaorigetu S, Wan G, Kaini R, et al. ApoL1, a BH3-only lipid-binding protein, induces autophagic cell death. Autophagy. 2008;4:1079–1082. [PubMed: 18927493]
22. Olabisi OA, Zhang JY, VerPlank L, et al. APOL1 kidney disease risk variants cause cytotoxicity by depleting cellular potassium and inducing stress-activated protein kinases. Proc Natl Acad Sci U S A. 2016;113:830–837. [PubMed: 26699492]
23. Cheng D, Weckerle A, Yu Y, et al. Biogenesis and cytotoxicity of APOL1 renal risk variant proteins in hepatocytes and hepatoma cells. J Lipid Res. 2015;56:1583–1593. [PubMed: 26089538]
24. Thomson R, Genovese G, Canon C, et al. Evolution of the primate trypanolytic factor APOL1. Proc Natl Acad Sci U S A. 2014;111:E2130–E2139. [PubMed: 24808134]
25. Lan X, Wen H, Lederman R, et al. Protein domains of APOL1 and its risk variants. Exp Mol Pathol. 2015;99:139–144. [PubMed: 26091559]
26. Wan G, Zhaorigetu S, Liu Z, et al. Apolipoprotein L1, a novel Bcl-2 homology domain 3-only lipid-binding protein, induces autophagic cell death. J Biol Chem. 2008;283:21540–21549. [PubMed: 18505729]
27. Beckerman P, Bi-Karchin J, Park AS, et al. Transgenic expression of human APOL1 risk variants in podocytes induces kidney disease in mice. Nat Med. 2017;23:429–438. [PubMed: 28218918]
28. Aghajan M, Booten SL, Althage M, et al. Antisense oligonucleotide treatment ameliorates IFN-gamma-induced proteinuria in APOL1-transgenic mice. JCI Insight. 2019;4:e126124. [PubMed: 31217349]
29. Bruggeman LA, Wu Z, Luo L, et al. APOL1-G0 or APOL1-G2 transgenic models develop preeclampsia but not kidney disease. J Am Soc Nephrol. 2016;27:3600–3610. [PubMed: 27026370]
30. Kruzel-Davila E, Shemer R, Ofir A, et al. APOL1-mediated cell injury involves disruption of conserved trafficking processes. J Am Soc Nephrol. 2017;28:1117–1130. [PubMed: 27864431]
31. Fu Y, Zhu JY, Richman A, et al. APOL1-G1 in nephrocytes induces hypertrophy and accelerates cell death. J Am Soc Nephrol. 2017;28:1106–1116. [PubMed: 27864430]
32. Madhavan SM, O'Toole JF, Konieczkowski M, et al. APOL1 variants change C-terminal conformational dynamics and binding to SNARE protein VAMP8. JCI Insight. 2017;2:e92581. [PubMed: 28724794]
33. Granado D, Muller D, Krausel V, et al. Intracellular APOL1 risk variants cause cytotoxicity accompanied by energy depletion. J Am Soc Nephrol. 2017;28:3227–3238. [PubMed: 28696248]
34. Ma L, Chou JW, Snipes JA, et al. APOL1 renal-risk variants induce mitochondrial dysfunction. J Am Soc Nephrol. 2017;28:1093–1105. [PubMed: 27821631]
35. Hayek SS, Koh KH, Grams ME, et al. A tripartite complex of suPAR, APOL1 risk variants and alphavbeta3 integrin on podocytes mediates chronic kidney disease. Nat Med. 2017;23:945–953. [PubMed: 28650456]
36. Giovinazzo JA, Thomson RP, Khalizova N, et al. Apolipoprotein L-1 renal risk variants form active channels at the plasma membrane driving cytotoxicity. Elife. 2020;9:e51185. [PubMed: 32427098]
37. Okamoto K, Rausch JW, Wakashin H, et al. APOL1 risk allele RNA contributes to renal toxicity by activating protein kinase R. Commun Biol. 2018;1:188. [PubMed: 30417125]

38. Wen H, Kumar V, Lan X, et al. APOL1 risk variants cause podocytes injury through enhancing endoplasmic reticulum stress. Biosci Rep. 2018;38. BSR20171713. [PubMed: 29967295]
39. Hermle T, Braun DA, Helmstadter M, et al. Modeling monogenic human nephrotic syndrome in the Drosophila garland cell nephrocyte. J Am Soc Nephrol. 2017;28:1521–1533. [PubMed: 27932481]
40. Lannon H, Shah SS, Dias L, et al. Apolipoprotein L1 (APOL1) risk variant toxicity depends on the haplotype background. Kidney Int. 2019;96:1303–1307. [PubMed: 31611067]
41. Weavers H, Prieto-Sanchez S, Grawe F, et al. The insect nephrocyte is a podocyte-like cell with a filtration slit diaphragm. Nature. 2009;457:322–326. [PubMed: 18971929]
42. Uzureau S, Lecordier L, Uzureau P, et al. APOL1 C-terminal variants may trigger kidney disease through interference with APOL3 control of actomyosin. Cell Rep. 2020;30:3821–3836.e3813. [PubMed: 32187552]
43. Chun J, Zhang JY, Wilkins MS, et al. Recruitment of APOL1 kidney disease risk variants to lipid droplets attenuates cell toxicity. Proc Natl Acad Sci U S A. 2019;116:3712–3721. [PubMed: 30733285]
44. Scales SJ, Gupta N, De Maziere AM, et al. Apolipoprotein L1-specific antibodies detect endogenous APOL1 inside the endoplasmic reticulum and on the plasma membrane of podocytes. J Am Soc Nephrol. 2020;31:2044–2064. [PubMed: 32764142]
45. Muller D, Schmitz J, Fischer K, et al. Evolution of renal-disease factor APOL1 results in cis and trans orientations at the endoplasmic reticulum that both show cytotoxic effects. Mol Biol Evol. 2021;38:4962–4976. [PubMed: 34323996]
46. Guida MC, Hermle T, Graham LA, et al. ATP6AP2 functions as a V-ATPase assembly factor in the endoplasmic reticulum. Mol Biol Cell. 2018;29:2156–2164. [PubMed: 29995586]
47. Zhang F, Zhao Y, Chao Y, et al. Cubilin and amnionless mediate protein reabsorption in Drosophila nephrocytes. J Am Soc Nephrol. 2013;24:209–216. [PubMed: 23264686]
48. Ryoo HD. Drosophila as a model for unfolded protein response research. BMB Rep. 2015;48:445–453. [PubMed: 25999177]
49. Adams CJ, Kopp MC, Larburu N, et al. Structure and molecular mechanism of ER stress signaling by the unfolded protein response signal activator IRE1. Front Mol Biosci. 2019;6:11. [PubMed: 30931312]
50. Ryoo HD, Domingos PM, Kang MJ, et al. Unfolded protein response in a Drosophila model for retinal degeneration. EMBO J. 2007;26:242–252. [PubMed: 17170705]
51. Bruno J, Pozzi N, Oliva J, et al. Apolipoprotein L1 confers pH-switchable ion permeability to phospholipid vesicles. J Biol Chem. 2017;292:18344–18353. [PubMed: 28918394]
52. Pant J, Giovinazzo JA, Tuka LS, et al. Apolipoproteins L1-6 share key cation channel-regulating residues but have different membrane insertion and ion conductance properties. J Biol Chem. 2021;297:100951. [PubMed: 34252458]
53. Schaub C, Verdi J, Lee P, et al. Cation channel conductance and pH gating of the innate immunity factor APOL1 are governed by pore-lining residues within the C-terminal domain. J Biol Chem. 2020;295:13138–13149. [PubMed: 32727852]
54. Hassan H, Tian X, Inoue K, et al. Essential role of X-box binding protein-1 during endoplasmic reticulum stress in podocytes. J Am Soc Nephrol. 2016;27:1055–1065. [PubMed: 26303067]

Translational Statement

Risk variants of the *APOL1* gene put millions of homozygous carriers at risk for kidney disease with an unclear pathogenesis. We apply transgenic expression of the gain-of-function risk variants in comparison with *APOL1* control variants in *Drosophila* podocyte-like nephrocytes and wing tissue. The *Drosophila* model facilitates a mechanistic analysis *in vivo*. Endoplasmic reticulum (ER) swelling and chaperone upregulation associated with the *APOL1* risk variants indicated ER stress. Genetic and pharmacologic inhibition of ER stress rescued *APOL1*-dependent cytotoxicity. These findings uncover an essential role of ER stress signaling and thus open avenues for the development of therapeutic strategies for *APOL1*-associated nephropathies.

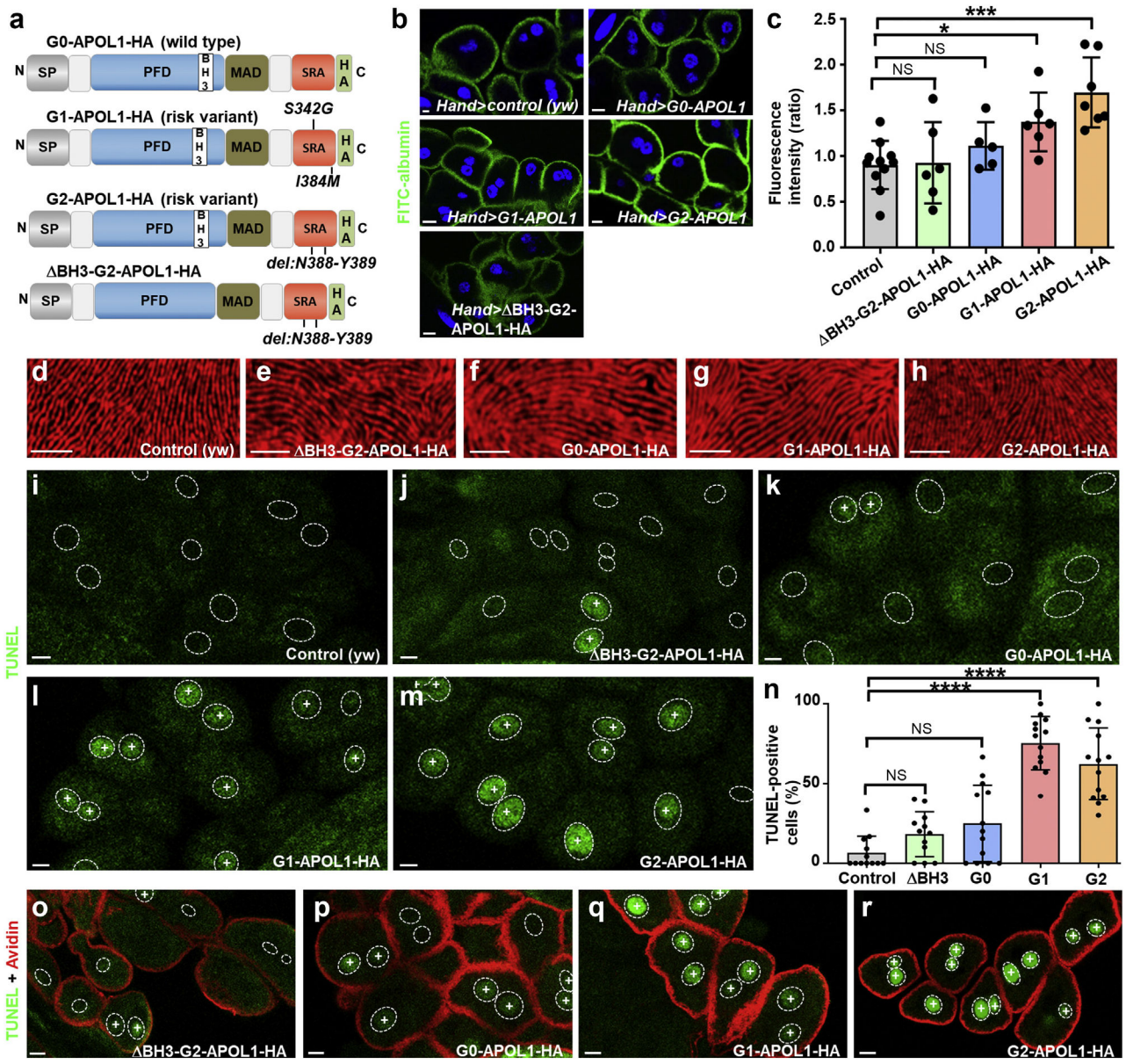

Figure 1 |. *APOL1* risk variants increase nephrocyte function and significantly increase the fraction of cells positive for the cell death marker terminal deoxynucleotidyl transferase–mediated dUTP nick end-labeling (TUNEL).

(**a**) Schematic indicating transgenic *APOL1* constructs employed in this study. The functional protein domains of *APOL1* encompass an N-terminal signal peptide that is followed by the pore forming domain (PFD), which harbors a BCL2 homology domain 3 (BH3). The PFD is followed by the membrane addressing (MAD) and finally the serum resistance antigen interacting domains (SRAs) before the C-terminus. All constructs carry an influenza hemagglutinin (HA) tag at the C-terminus unless otherwise indicated. G0-*APOL1* represents a wild-type *APOL1* sequence (top), whereas G1-*APOL1* carries 2 missense variants (p.S342G and p.I384M) and G2-APOL1 a deletion of 2 amino acids (del: N388/Y389). ΔBH3-G2-*APOL1* (bottom) carries an additional short deletion (del: L158-Q166) within the BH3 domain and is otherwise identical with G2-*APOL1.* Deletion

of these residues has been shown to abrogate toxicity in cultured human cells,[25] so we chose this as a control variant. (**b**) Expression of *APOL1* risk variants G1-*APOL1* and G2-*APOL1,* but not expression of **Δ**BH3-G2-*APOL1* and G0-*APOL1* in *Drosophila* garland cell nephrocytes using *Hand*-GAL4 increases uptake of fluorescein isothiocyanate–albumin as an established assay of nephrocyte function. Flies were raised at 29 °C. Nuclei are marked by Hoechst 33342 in blue here and throughout the figure. (**c**) Quantitation of data in (**b**); mean fluorescence per animal based on the 3 brightest cells in ratio to control experiment is shown; n = 6–11 animals per genotype; $P < 0.05$ for G1-APOL1 and $P < 0.001$ for G2-APOL1). (**d–h**) Tangential sections of control garland cell nephrocytes (**d**) or garland cell nephrocytes expressing **Δ**BH3-G2-*APOL1* (**e**), G0-*APOL1* (**f**), G1-*APOL1* (**g**), or G2-*APOL1* (**h**), using *Hand-GAL4* at 29 °C are shown. Cells are stained for KIRREL/NEPH1 ortholog Kirre (red), revealing an unaffected staining pattern of slit diaphragms for all indicated genotypes. (**b, i–m, o–r**) Bar = 10 μm. (**d–h**) Bar = 5 μm. (**i–m**) TUNEL labeling of garland cell nephrocytes from third instar larvae is shown for the indicated genotypes, and positivity is indicated by an intranuclear "+." Outlines of nuclei are shown by dotted circles based on Hoechst 33342 staining (data not shown). (**i**) In control animals (*dKlf15-GAL4*/+), TUNEL-positive nephrocytes are rare or absent. TUNEL-positive cells become slightly more frequent with expression of control protein **Δ***BH3-G2-APOL1* (**j**) and wild-type *G0-APOL1* (**k**). In contrast, the risk variants *G1-APOL1* (**l**) and *G2-APOL1* (**m**) caused a high fraction of TUNEL-positive cells. (**n**) Quantitation of data in (**i–m**); the fraction of TUNEL-positive cells is shown (percentage); n = 12 to 15 animals per genotype; $P > 0.05$ for **Δ**BH3-*G2-APOL1* and *G0-APOL1,* and $P < 0.001$ for G1- and G2-*APOL1* compared with control animals. (**o–r**) Shown are nephrocytes that were exposed to red fluorescent tracer Texas Red–avidin as a readout of nephrocyte function followed by TUNEL staining. TUNEL-positive nephrocytes show an equal uptake compared with TUNEL-negative neighboring cells in **Δ***BH3-G2-APOL1* (**o**) and *G0-APOL1* (**p**) expressing cells. Increased endocytosis of Texas Red–avidin is observed in G1-*APOL1* (**q**) and G2-*APOL1* (**r**) expressing nephrocytes despite widespread TUNEL positivity. NS, not significant. To optimize viewing of this image, please see the online version of this article at www.kidney-international.org.

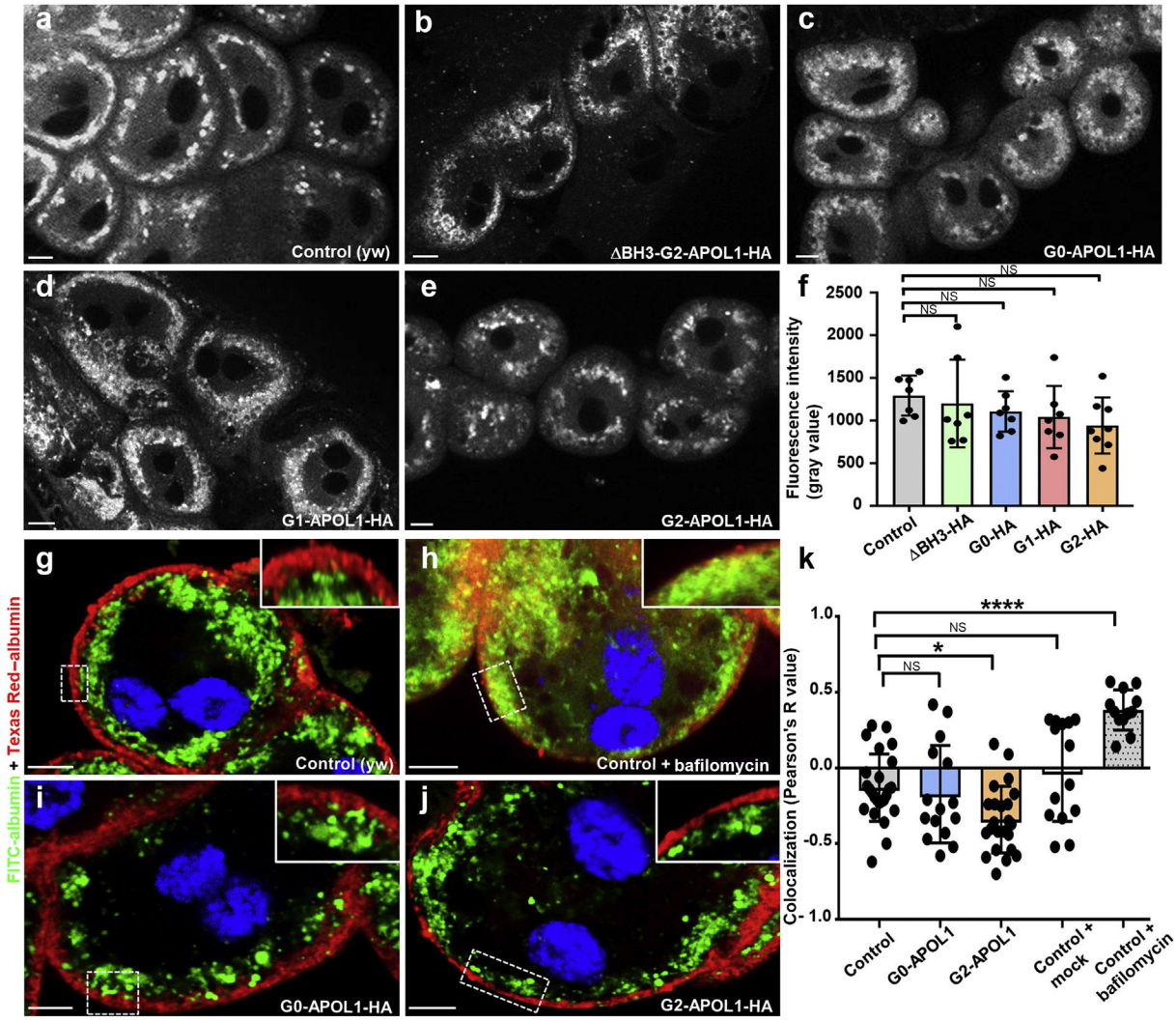

Figure 2 |. Expression of *APOL1* risk variants in garland cell nephrocytes does not reduce lysotracker staining and induces no overt defect in endocytosis.

(**a–e**) Confocal live cell imaging of garland cell nephrocytes dissected from third instar larvae reveals acidic vesicles because the living cells were exposed to Lysotracker Red DND-99 at 0.25 μM for 5 minutes before immediate recording. Fluorescence intensity of the indicated genotypes appears comparable. (**f**) Quantitation of dye-derived fluorescence intensity from data analogous to (**a–e**), expressed as mean fluorescence intensity per animal, indicates no significant difference compared with control animals (Hand-GAL/+) for any *APOL1* variant studied here (n = 7–8; $P > 0.05$ for all indicated genotypes). (**g–j**) Shown are nephrocytes that were exposed to 2 consecutive tracers *ex vivo*. First fluorescein isothiocyanate (FITC)–albumin (green) followed by chase period and finally Texas Red–albumin (red). Note how both tracers become spatially separated through endocytic progressing and progression toward late endosomes in control cells (*Hand-GAL4*/+) (**g**), whereas a block of endolysosomal acidification results in a partial colocalization (**h**). In contrast, expression of G0-*APOL1* (**i**) and G2-*APOL1* (**j**) did not induce colocalization, suggesting a largely unimpaired processing of endocytic cargo. Flies were raised at 29 °C.

(**k**) Quantitation of data analogous to (**g**–**j**) using Pearson's coefficient (3 individual cells each from 4–8 animals are shown per genotype; $P < 0.05$ for G2-*APOL1* and $P < 0.0001$ for bafilomycin treatment). Pearson's coefficient ranges from +1 (perfect colocalization) to −1 (perfect separation). With G2-*APOL1,* the separation becomes even more pronounced, suggesting swifter endocytic processing. Bafilomycin is the only condition that delays endocytic processing. NS, not significant. To optimize viewing of this image, please see the online version of this article at www.kidney-international.org.

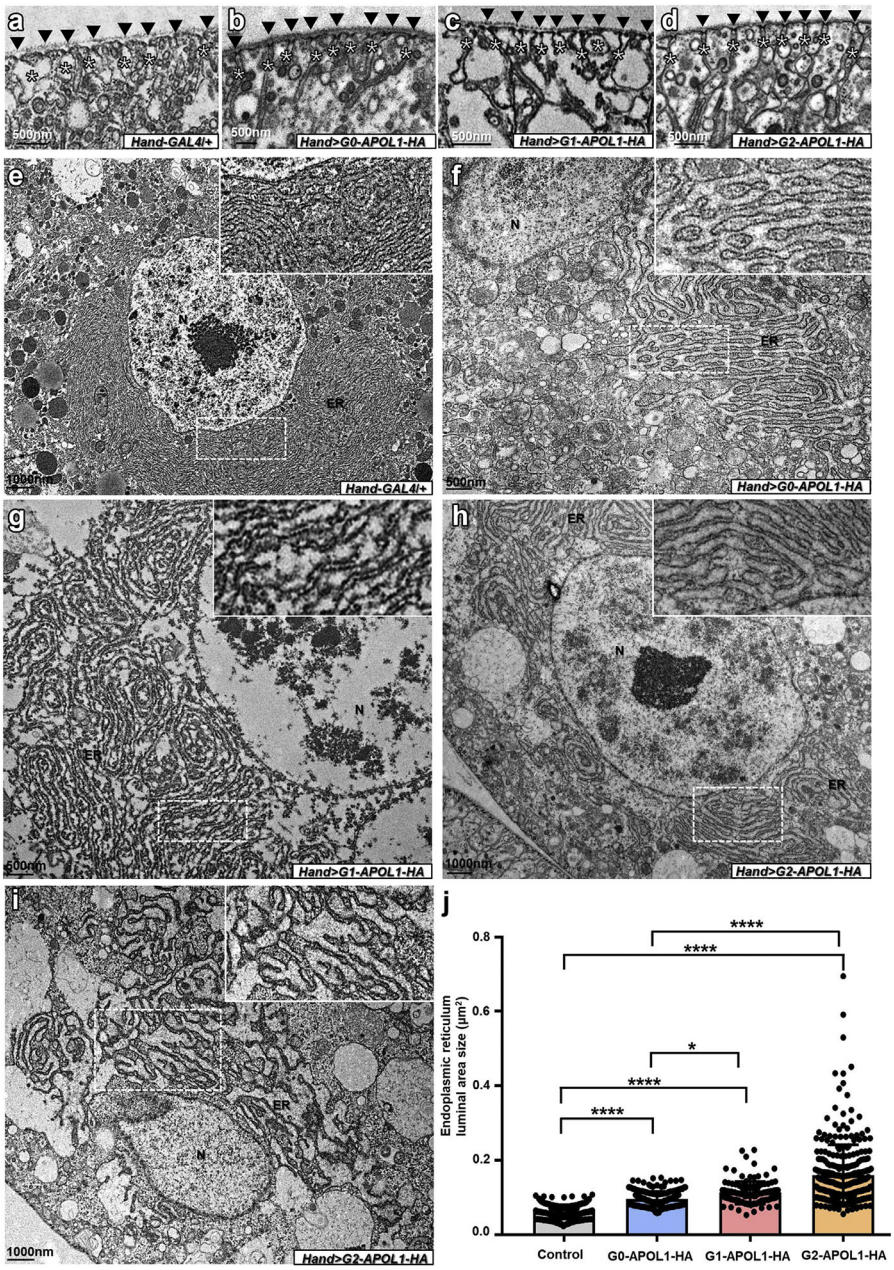

Figure 3 |. *APOL1* expression has no effect on slit diaphragms but induces endoplasmic reticulum (ER) swelling in *Drosophila* nephrocytes.

(**a–d**) Transmission electron microscopy images of garland cell nephrocytes dissected from third instar larvae are shown. (**a**) Control nephrocytes (*Hand-GAL4/+*) show regular formation of slit diaphragms (black arrowheads) and the membrane invaginations called labyrinthine channels (asterisks). Labyrinthine channels seem slightly more slender on expression of G0-*APOL1* (**b**), G1-*APOL1* (**c**), and G2-*APOL1* (**d**). All flies were raised at 29 °C. (**e**) Overview of a control nephrocyte that shows regular size of the extensive ER in control garland cell nephrocytes (*Hand-GAL4/+*). Nuclei are indicated by the letter N. (**f**) Mild swelling of the ER occurs on expression of G0-*APOL1* using *Hand-GAL4.* (**g–i**) Expression of risk variants G1-*APOL1* (**g**) and G2-*APOL1* (**h**) causes more pronounced or

ER swelling. For some animals expressing G2-*APOL1*, even more severe ER swelling could be observed (**i**). (**j**) Quantitation from electron microscopic images analogous to (**g–i**) was performed by measuring the area of a single ER lumen for a distance of 1 μm for 20 adjacent ER lumina per cell. The results confirm a significant increase of ER swelling for risk variants G1-*APOL1* and G2-*APOL1* compared with wild-type G0-*APOL1* and any APOL1 variant compared with wild-type control (*Hand-GAL4/+*; n = 20 representative distances per cell each for 3–5 cells from 4–5 animals per genotype; $P < 0.0001$ for G2-*APOL1* vs. G0-*APOL1*, $P < 0.05$ for G1-*APOL1* vs. G0-*APOL1*, $P < 0.0001$ for G0-*APOL1* vs. control, $P < 0.0001$ for G1-*APOL1* vs. control, and $P < 0.0001$ for G2-*APOL1* vs. control). To optimize viewing of this image, please see the online version of this article at www.kidney-international.org.

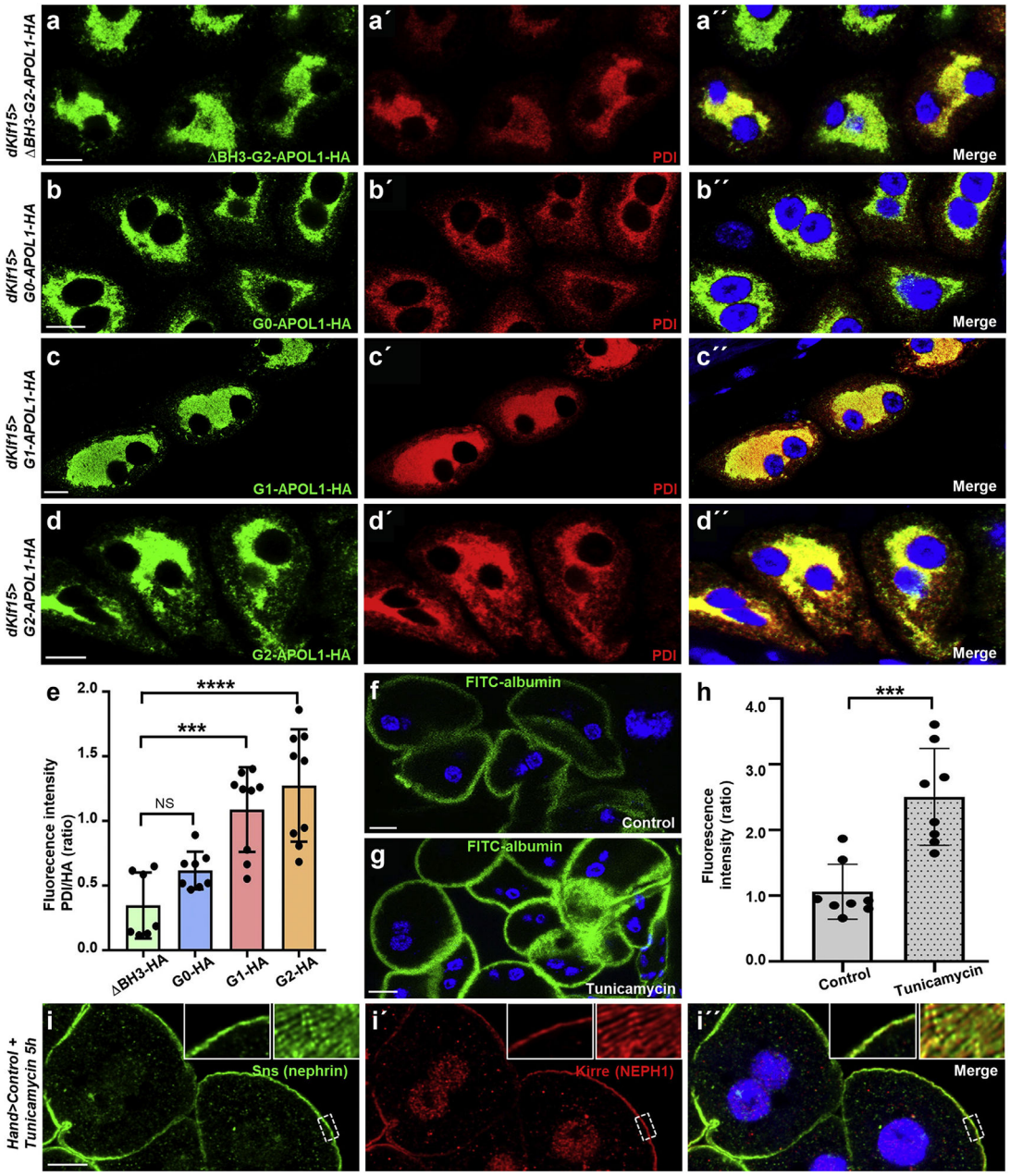

Figure 4 |. Endoplasmic reticulum (ER) resident *APOL1* risk variants induce ER stress in nephrocytes.

(**a–d**″) Shown are equatorial cross-sections of garland cell nephrocytes from third instar larvae expressing various *APOL1* transgenes under control of *dKlf15-GAL4.* Cells are costained for HA to visualize the tagged transgenes and the ER marker/ER stress response target gene PDI. All transgenes show complete colocalization with the ER marker, including ΔBH3-G2-*APOL1* (**a–a**″), G0-*APOL1* (**b–b**″), G1-*APOL1* (**c–c**″), and G2-*APOL1* (**d–d**″). The renal risk variants reveal an enhanced signal from the protein disulfide-isomerase (PDI) antibody, suggesting a greater abundance of PDI as a result of ER stress induction. All flies were raised at 29 °C. Bar = 10 μm, and nuclei are marked by Hoechst 33342 in blue here and throughout the figure. (**e**) Quantitation of fluorescence intensity of signal derived from PDI

staining is shown for confocal images analogous to (**a–d**). For quantitation, the fluorescence intensity of PDI was measured within the area of the cell that was strongly hemagglutinin (HA) positive. Wild-type and renal risk variants are compared with the control transgene **Δ**BH3-G2-*APOL1* (n = 7–9; $P > 0.05$ for G0-*APOL1,* $P < 0.001$ for G1-*APOL1,* and $P < 0.0001$ for G2-*APOL1*). (**f,g**) Shown is fluorescein isothiocyanate (FITC)–albumin endocytosis after 30 seconds exposure as readout of nephrocyte function for garland cell nephrocytes from control animals exposed to ER stress inducer tunicamycin or vehicle control (dimethylsulfoxide). Exposure to ER stress inducer tunicamycin for 5 hours results in increased uptake of FITC-albumin (**g**) compared with treatment with vehicle alone (**f**). (**h**) Quantitation of data in (**f**) through (**g**) (mean fluorescence per animal in ratio to control experiment is shown; n = 8 animals per condition; $P < 0.001$). (**i–i″**) Equatorial cross-section of wild-type garland cell nephrocytes dissected from a larva treated with tunicamycin for 5 hours shows regular staining pattern of the slit diaphragm proteins Sns (green) and Kirre (red). Insets show a magnified detail of slit diaphragms (left) and tangential sections revealing the regular fingerprint-like staining pattern (right). Bar = 10 μm, and nuclei are marked by Hoechst 33342 in blue here. Flies were raised at 29 °C. To optimize viewing of this image, please see the online version of this article at www.kidney-international.org.

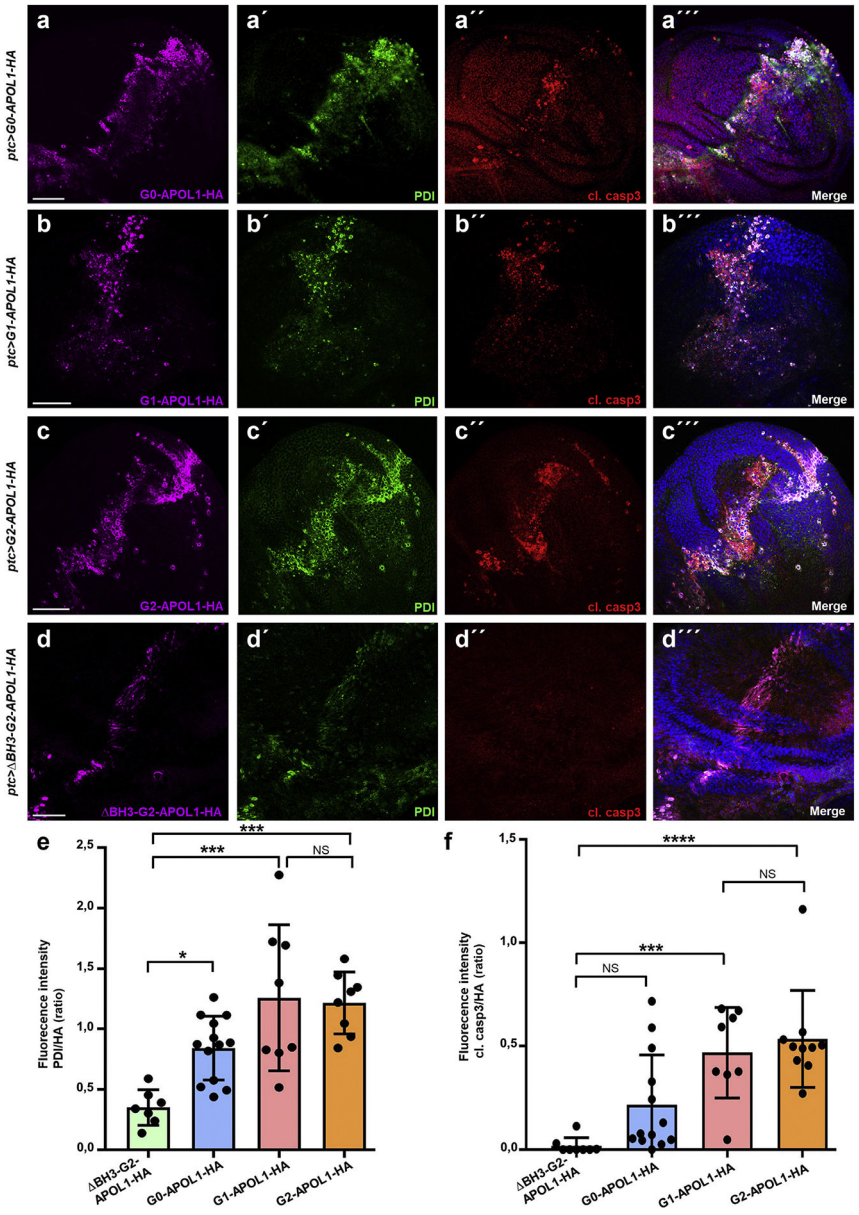

Figure 5 |. *APOL1* risk variants trigger endoplasmic reticulum (ER) stress and cell death in the *Drosophila* wing imaginal disc.

(**a–d‴**) Shown are confocal images of third instar wing imaginal discs costained for hemagglutinin (HA) to detect the APOL1 transgenes, ER marker protein disulfide-isomerase (PDI) to reveal ER stress induction, and cleaved caspase-3 (cl. casp3) to identify apoptotic cells. Transgenes are expressed under control of *ptc-GAL4* at 18 °C. Expression occurs in a slightly tilted vertical strip that traverses the center of the wing disc. On expression of G0-*APOL1* (**a–a‴**), the transgenic protein is accompanied by mild upregulation of PDI. The expression domain further shows interspersed apoptotic cells. Expression of risk variants G1-*APOL1* (**b–b‴**) and G2-*APOL1* (**c–c‴**) entails a more pronounced ER stress and cell death induction, whereas ΔBH3-G2-*APOL1* (**d–d‴**) results in weak PDI increase without induction of cell death. Bar = 50 μm, and nuclei are marked by Hoechst 33342 in blue

here and throughout the figure. (**e**) Quantitation of data analogous to (**a–d**) for fluorescence intensity of PDI staining in ratio to the expression strength indicated by the HA signal (n = 8–13 per genotype; **P** < 0.05 for G0-*APOL1, P* < 0.001 for G1-*APOL1,* and *P* < 0.001 for G2-*APOL1* comparing the respective construct vs. **Δ**BH3-G2-*APOL1* as the control transgene). (**f**) Quantitation of data analogous to (**a–d**) for fluorescence intensity of cleaved caspase-3 staining in ratio to the expression strength indicated by the HA signal. Only the expression of the renal risk variants G1- and G2-*APOL1* result in a significant extent of apoptotic cells (n = 8–12; *P* > 0.05 for G0-*APOL1, P* < 0.001 for G1-*APOL1,* and *P* < 0.0001 for G2-*APOL1* comparing each construct vs. **Δ**BH3-G2-*APOL1* as the control transgene). NS, not significant. To optimize viewing of this image, please see the online version of this article at www.kidney-international.org.

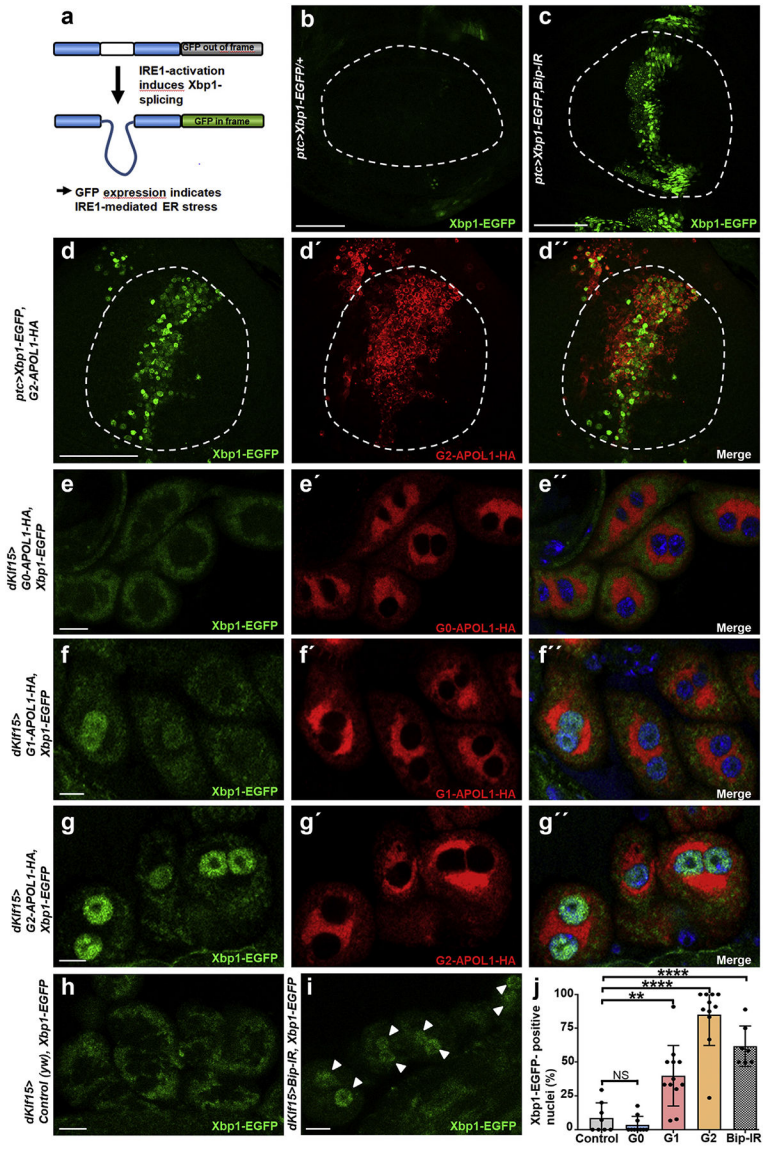

Figure 6 |. *APOL1* risk variants trigger *IRE1*-dependent endoplasmic reticulum (ER) stress.

(**a**) Schematic indicates function of the *Xbp1*–enhanced green fluorescent protein (EGFP) reporter. EGFP expression depends on activation of *IRE1* that shifts the reading-frame. (**b,c**) Expression of EGFP in the wing pouch (circle) is absent in control animals (**b**) but becomes detectable on direct activation of ER stress through expression of *bip*-RNAi by *ptc-GAL4* (**c**). Bar = 50 μm. (**d–d″**) Expression of G2-*APOL1* with *ptc-GAL4* induces expression of *Xbp1*-EGFP, a reporter of *Ire1*-dependent ER stress. Hemagglutinin (HA) staining indicates G2-*APOL1* expression. Bar = 50 μm. (**e–e″**) Expression of wild-type G0-*APOL1* with *dKlf15-GAL4* at 29 °C lacks significant expression of the ER stress reporter *Xbp1*-EGFP in garland cell nephrocytes. Nuclei are marked by Hoechst 33342 in blue. Bar = 10 μm. (**f–g″**) Expression of the renal risk variants G1-*APOL1-HA* (**f–f″**) and G2-*APOL1-HA* (**g–g”**) at 29 °C in garland cell nephrocytes results in EGFP-derived fluorescence within the nucleus, indicating induction of *IRE1*-dependent ER stress. Nuclei are marked by Hoechst 33342 in blue. (**h**) Lack of nuclear EGFP-derived fluorescence in control nephrocytes (*yw*) at 29

°C shows that ER stress is not constitutively active in garland cell nephrocytes during the larval stage. Bar = 10 μm. Nuclei are marked by Hoechst 33342 (data not shown). (**i**) Direct induction of ER stress through expression of *Bip-RNAi* at 29 °C as positive control results in appearance of EGFP-derived fluorescence within the nuclear area (arrowheads). Bar = 10 μm. Nuclei are marked by Hoechst 33342 (data not shown). (**j**) Quantitation of data analogous to (**e–i**) for the fraction of *XBP1*–EGFP-positive nuclei confirms a significant induction of the ER stress reporter for the risk variants and the positive control *Bip-RNAi* (n = 7–12 per condition; $P > 0.05$ for G0-*APOL1,* $P < 0.01$ for G1-*APOL1,* and $P < 0.0001$ for G2-*APOL1* and *Bip-RNAi* comparing each construct with control [*yw*]). To optimize viewing of this image, please see the online version of this article at www.kidney-international.org.

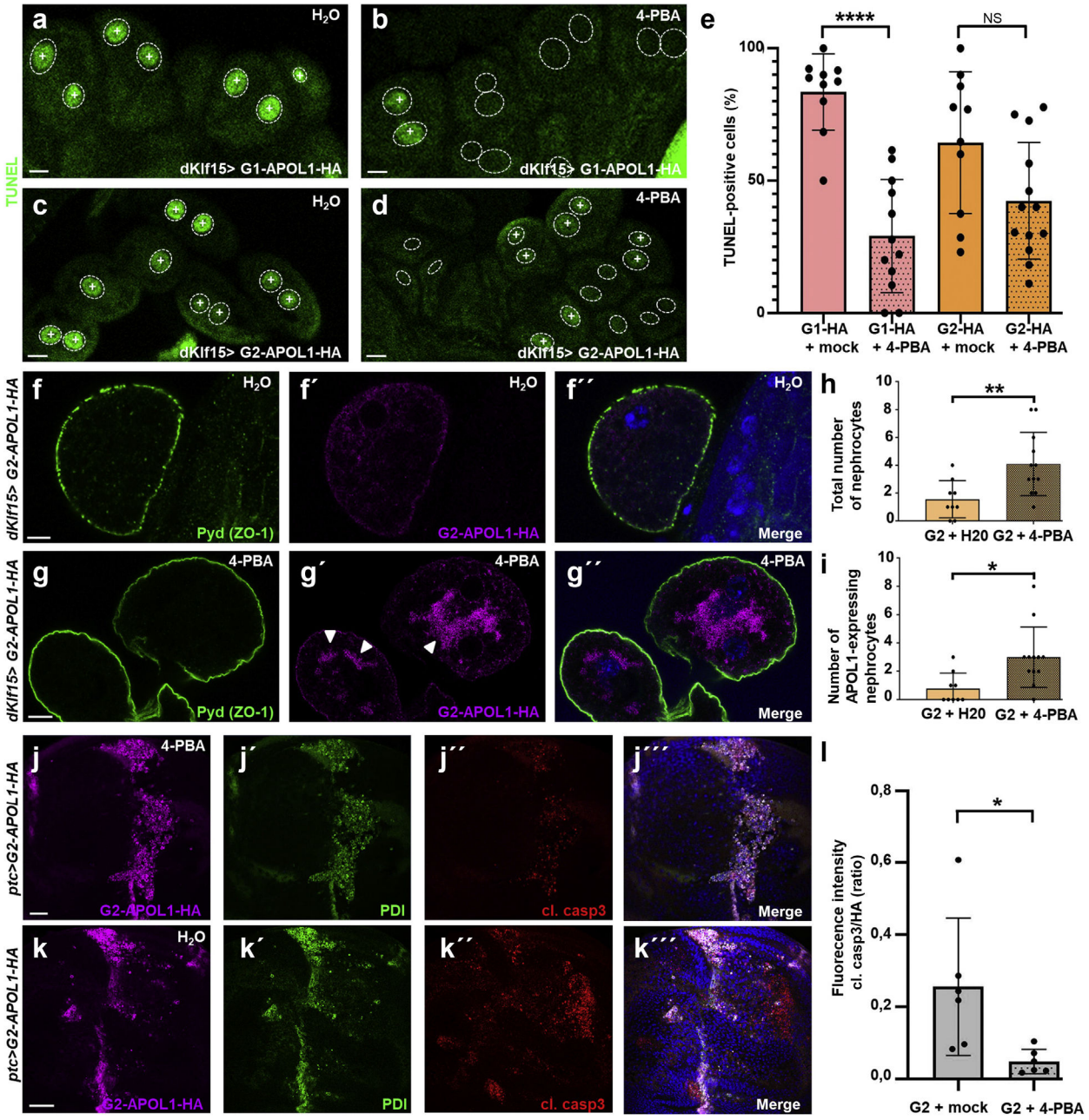

Figure 7 |. *G2-APOL1*–dependent cell death is blunted by pharmacologic inhibition of endoplasmic reticulum (ER) stress.

(**a–d**) Terminal deoxynucleotidyl transferase–mediated dUTP nick end-labeling (TUNEL) labeling of garland cell nephrocytes from third instar larvae is shown for G1-*APOL1* (**a,b**) and G2-*APOL1* (**c,d**). Animals were raised in liquid for 24 hours containing 4 mM 4-phenylbutyric acid (4-PBA; **b,d**) or vehicle alone (H_2O; **a,c**). TUNEL positivity is indicated by an intranuclear "+." Outlines of nuclei are shown by dotted circles based on Hoechst 33342 staining (data not shown). Note that TUNEL-positive cells become less abundant on 4-PBA treatment. Bar = 10 μm. (**e**) Quantitation of data analogous to (**a–d**); the fraction of TUNEL-positive cells is shown (percentage); n = 10 to 13 animals per genotype

and condition. $P < 0.0001$ for G1-*APOL1* and $P > 0.05$ for G2-*APOL1* comparing 4-PBA with control treatment. (**f–g″**) Larvae expressing *G2-APOL1* under control of *dKlf15-GAL4* were fed with yeast with addition of vehicle alone (H_2O; **f–f″**) or 4 mM 4-PBA (g–g") for ~48 hours before reaching puparium. After eclosure, adult animals were dissected to stain adult nephrocytes for slit diaphragm protein polychaetoid (pyd) and HA tag. After mock treatment (H_2O), nephrocyte numbers were reduced on G2-*APOL1* expression (compare Supplementary Figure S2E and F) and surviving nephrocytes mostly showed downregulation of the transgene (the typical situation with exclusively nonexpressing nephrocyte is shown in **f–f″**). In contrast, treatment with 4-PBA increased the number of surviving nephrocytes, further resulting in a higher number of cells expressing *G2-APOL1* (**g–g″**). Bars = 10 μm. (**h**) Quantitation of data analogous to (**f–g″**) for the total number of nephrocytes per adult animal shows significant increase after attenuation of ER stress using 4-PBA (n = 8–12 per condition; $P < 0.01$). (**i**) Quantitation of data analogous to (**f–g″**) for the number of nephrocytes positive for HA signal, indicating transgene expression per adult animal shows significant increase after attenuation of ER stress using 4-PBA (n = 9–12 per condition; $P < 0.05$). (**j–k‴**) Larvae expressing G2-*APOL1* using *ptc-GAL4* in the wing disc were exposed to ER stress inhibitor 4-PBA in liquid food for 24 hours. Confocal imaging of wing disc after treatment reveals mild residual upregulation of protein disulfide-isomerase (PDI) and strongly reduced induction of apoptosis indicated by cleaved caspase-3 (cl. casp3). Pharmacologic inhibition of ER stress induction thus partially blocks induction of apoptosis associated with G2-APOL1 (**j–j‴**). Larvae expressing *G2-APOL1* under *ptc-GAL4* after treatment with vehicle alone (H_2O) in liquid food for 24 hours show robust upregulation of PDI and numerous cells that are positive for cleaved caspase-3 (**j–k‴**). Nuclei are marked by Hoechst 33342 in blue here. Bar = 50 μm. (**l**) Quantitation of data in (**j–k‴**) for fluorescence intensity of cleaved caspase-3 staining in ratio to the expression strength indicated by the HA signal shows significant reduction of cleaved caspase-3 signal (n = 6 per condition; $P < 0.05$). NS, not significant. To optimize viewing of this image, please see the online version of this article at www.kidney-international.org.

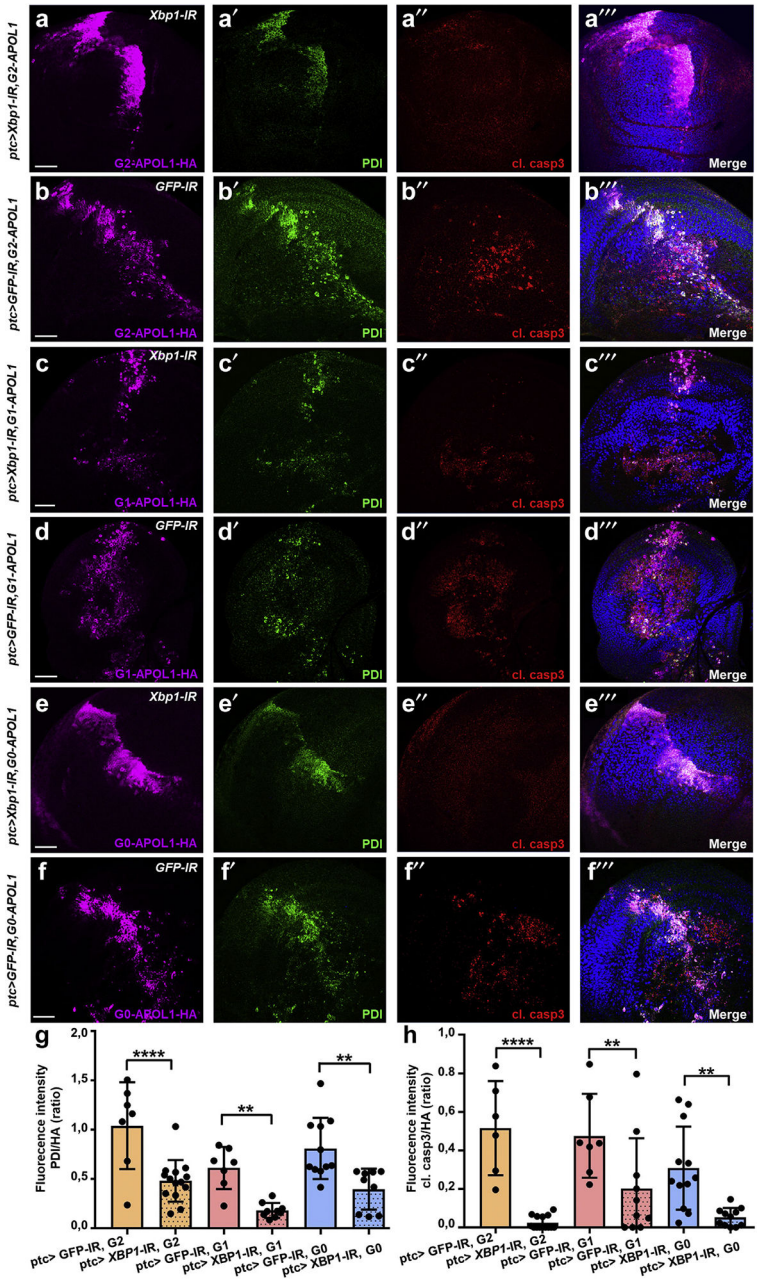

Figure 8 |. *APOL1*-dependent cell death is abrogated by inhibition of *IRE1*-mediated endoplasmic reticulum (ER) stress.

(**a**–**f**″) Coexpression of *Xbp1*–RNA interference (RNAi) to block IRE1-dependent ER stress is compared with green fluorescent protein (GFP)–RNAi as control knockdown for concomitant expression of *APOL1* variants, as indicated in wing imaginal discs from third instar larvae. Discs are stained for hemagglutinin (HA) to distinguish APOL1 transgenes, protein disulfide-isomerase (PDI) to identify the ER stress response, and cleaved caspase-3 (cl. casp3) to detect cell death. *Xbp1*-RNAi expression (rescue; **a**, **c**, and **e**) allowed *APOL1* transgene expressing animals to be raised at 25 °C; crosses with *APOL1* transgenes together with GFP-RNAi (nonrescue; **b**, **d**, and **f**) had to be run at 18 °C as higher temperatures

(causing stronger APOL1 transgene expression) were precluded by lethality. Inhibition of the *IRE1*-dependent branch of ER stress signaling by *Xbp1*-RNAi attenuated upregulation of PDI and induction of cell death (cleaved caspase-3) for G2-*APOL1* (**a,b**), G1-*APOL1* (**c,d**), and G0-*APOL1* (**e,f**). Bars = 50 μm, and nuclei are marked by Hoechst 33342 in blue. (**g**) Quantitation of data analogous to (**a–f‴**) for fluorescence intensity of PDI staining in ratio to the expression strength indicated by the HA signal (n = 7–14 per genotype; $P <$ 0.0001 for G2-*APOL1,* $P < 0.01$ for G1-*APOL1,* and $P < 0.01$ for G0-*APOL1* comparing rescue [Xbp1-RNAi] vs. nonrescue [GFP-RNAi]). Inhibition of the IRE1-dependent branch thus diminishes *APOL1*-dependent upregulation of the ER stress response target PDI. (**h**) Quantitation of data analogous to (**a–f‴**) for fluorescence intensity of cleaved caspase-3 staining in ratio to the expression strength indicated by the HA signal (n = 7–14 per genotype; $P < 0.0001$ for G2-*APOL1,* $P < 0.01$ for G1-*APOL1,* and $P < 0.01$ for G0-*APOL1* comparing rescue [Xbp1-RNAi] vs. nonrescue [GFP-RNAi]). Inhibition of the *IRE1*-dependent branch thus blocks *APOL1*-dependent cell death. To optimize viewing of this image, please see the online version of this article at www.kidney-international.org.